© 2022. Published by The Company of Biologists Ltd | Journal of Cell Science (2023) 136, jcs259969. doi:10.1242/jcs.259969

RESEARCH ARTICLE

SPECIAL ISSUE: CELL BIOLOGY OF MOTORS

Actin turnover protects the cytokinetic contractile ring from structural instability

Zachary McDargh, Tianyi Zhu, Hongkang Zhu and Ben O'Shaughnessy*

ABSTRACT

In common with other actomyosin contractile cellular machineries, actin turnover is required for normal function of the cytokinetic contractile ring. Cofilin is an actin-binding protein contributing to turnover by severing actin filaments, required for cytokinesis by many organisms. In fission yeast cofilin mutants, contractile rings suffer bridging instabilities in which segments of the ring peel away from the plasma membrane, forming straight bridges whose ends remain attached to the membrane. The origin of bridging instability is unclear. Here, we used molecularly explicit simulations of contractile rings to examine the role of cofilin. Simulations reproduced the experimentally observed cycles of bridging and reassembly during constriction, and the occurrence of bridging in ring segments with low density of the myosin II protein Myo2. The lack of cofilin severing produced ∼2-fold longer filaments and, consequently, ∼2-fold higher ring tensions. Simulations identified bridging as originating in the boosted ring tension, which increased centripetal forces that detached actin from Myo2, which was anchoring actin to the membrane. Thus, cofilin serves a critical role in cytokinesis by providing protection from bridging, the principal structural threat to contractile rings.

KEY WORDS: Cytokinesis, Contractile ring, ADF/cofilin family, Actin turnover, Instability

INTRODUCTION

Turnover of actin and other components is a universal feature of actomyosin contractile machineries in cells. Actin turns over through nucleation of filamentous actin by formins, Arp2/3 or other factors (Pollard, 2007), and by dissociation and/or disassembly of filaments. Cofilin is an actin-binding protein whose severing activity is critical for actin turnover in many machineries (Elam et al., 2013), including the actomyosin contractile ring that drives cell division during cytokinesis (D'Avino et al., 2015; Pollard and O'Shaughnessy, 2019; Pollard and Wu, 2010). Cofilin is required for cytokinesis in many organisms (Abe et al., 1996; Gunsalus et al., 1995; Ono et al., 2003) including fission yeast (Nakano and Mabuchi, 2006), but many aspects of the mechanisms that make cofilin essential to cytokinesis remain poorly understood.

Fission yeast (*Schizosaccharomyces pombe*) assembles a contractile ring from several hundred precursor protein complexes called nodes, each node incorporating the myosin II Myo2, the formin Cdc12, which nucleates and grows actin filaments, and other components (Wu et al., 2006). Normal ring assembly requires cofilin (Adf1), as shown by studies of cytokinesis with mutants (Chen and Pollard, 2011; Nakano and Mabuchi, 2006). In cofilin mutants with reduced actin binding and severing activity, contractile rings failed to assemble normally from nodes, but instead assemble rings more slowly via diverse intermediate structures (Chen and Pollard, 2011). It has been argued (Chen and Pollard, 2011) that cofilin-mediated actin filament severing is required for assembly from the nodes, which are pulled together by pairwise actin filament connections that need regular renewal by severing to avoid node clumping and assembly failure (Vavylonis et al., 2008).

The role of cofilin during constriction of the assembled ring is much less clear. Is cofilin needed for constriction, and if so what is the mechanism? Fission yeast contractile rings in cells with cofilin mutations constricted at normal mean rates, but with more variability (Chen and Pollard, 2011). However, during constriction, rings exhibited remarkable structural irregularities in which segments of the ring peeled away from the plasma membrane into straight segments we call bridges (Cheffings et al., 2019; Chen and Pollard, 2011; Malla et al., 2022). As bridging tended to occur in ring segments with lower Myo2 density, it has been suggested that the instability originated in a combination of reduced local Myo2-mediated actin anchoring and reduced local ring tension in the bridging region (Cheffings et al., 2019).

The contractile ring is a complex cellular machine of many components, so understanding the mechanisms of constriction and force production can benefit from mathematical modeling (Glotzer, 2005; O'Shaughnessy and Thiyagarajan, 2018; Pollard and O'Shaughnessy, 2019). Fission yeast is uniquely positioned for realistic quantitative modeling due to a wealth of available data on the identities, amounts, biochemical properties and organization of ring components (Chatterjee and Pollard, 2019; Chen et al., 2015; Courtemanche et al., 2016; Friend et al., 2018; Hayakawa et al., 2020 preprint; Pollard et al., 2017; Pollard and Wu, 2010; Stark et al., 2010; Takaine et al., 2015; Wu and Pollard, 2005). This data has been used to constrain models of the contractile ring that reproduced structural features and ring tensions measured in live cells (Alonso-Matilla et al., 2019; McDargh et al., 2021 preprint; Stachowiak et al., 2014; Thiyagarajan et al., 2017). In contrast to the classic sarcomeric force production mechanism of striated muscle (Huxley and Niedergerke, 1954; Huxley and Hanson, 1954), a sliding node mechanism emerged, where Myo2 and the unconventional myosin Myp2 (Bezanilla et al., 1997) pull nodes around the ring through attached actin filaments barbed-end-anchored to nodes via formins (McDargh et al., 2021 preprint). This generates tension in filaments, and a net ring tension. Experimental and modeling studies of septation, the growth of new cell wall in the wake of the constricting ring, suggest septation determines the constriction rate, whereas the centripetal force from the ring mechanically regulates septation (Thiyagarajan et al., 2015; Zhou et al., 2015).

Department of Chemical Engineering, Columbia University, New York, NY 10027, USA.

*Author for correspondence (bo8@columbia.edu)

Z.M., 0000-0001-9022-5593; B.O., 0000-0003-4223-3489

Handling Editor: Michael Way
Received 25 February 2022; Accepted 17 August 2022

Journal of Cell Science (2023) 136, jcs259969. doi:10.1242/jcs.259969

Here, we used mathematical modeling to study the role of cofilin-mediated turnover in constricting contractile rings. Using a well-tested simulation framework (McDargh et al., 2021 preprint), we studied fission yeast contractile rings with the ADF-M3 cofilin mutant, which has reduced actin binding and severing activity (Chen and Pollard, 2011). Simulations quantitatively reproduced the experimentally observed bridges, the correlation with lower Myo2 densities and, remarkably, the cyclic character of bridging with three bridging–re-healing episodes during the course of constriction (Cheffings et al., 2019). The origin of the bridging instability is that actin filaments grow much longer without cofilin-mediated severing, so the ring tension is massively boosted, sufficient to pull actin filaments away from the Myo2 that anchors them to the membrane. In live cells (Laplante et al., 2015) and in simulations (McDargh et al., 2021 preprint), essentially the same bridging instability is seen in *myo2-E1* mutants with weakened binding to actin, showing that either increased centripetal loading or reduced anchoring provokes bridging. Thus, by maintaining actin filament lengths within a safe boundary, cofilin protects the contractile ring from bridging instability, the principal structural threat to the contractile ring.

RESULTS

Molecularly explicit simulation of the fission yeast cytokinetic ring

To examine the role of cofilin, we adapted a molecularly explicit model of the fission yeast contractile ring we developed previously (McDargh et al., 2021 preprint). The model represents the molecules in the ring using coarse-grained schemes, necessary to simulate the large number of molecules and long timescales involved, and is highly constrained by extensive experimental data that makes the fission yeast contractile ring presently the most amenable to realistic mathematical modeling. Our model incorporates the measured amounts, turnover rates and biochemical properties of key components, and their organization in the ring. The amounts of many ring components were measured over time and many were biochemically characterized (Chatterjee and Pollard, 2019; Chen et al., 2015; Courtemanche et al., 2016; Friend et al., 2018; Hayakawa et al., 2020 preprint; Pollard et al., 2017; Pollard and Wu, 2010; Stark et al., 2010; Takaine et al., 2015; Wu and Pollard, 2005). Super-resolution fluorescence photoactivation localization microscopy (FPALM) showed the actomyosin organization in constricting rings is built from protein complexes called nodes (Laplante et al., 2016), anchored to the plasma membrane (PM). Each node contains the myosin II protein Myo2, the actin filament nucleator formin Cdc12 and other components (Laplante et al., 2016; McDonald et al., 2017; Vavylonis et al., 2008; Wu et al., 2006). A second unconventional myosin II Myp2 does not belong to the nodes and is likely unanchored from the plasma membrane.

Here, we briefly summarize the main points of the model (for details and parameter values, see Materials and Methods and McDargh et al., 2021 preprint). In the model, each node is a coarse-grained representation of the organization revealed by FPALM, including Myo2 and Cdc12 (Laplante et al., 2016) (Fig. 1A). Dimers of the formin Cdc12 bind the node and nucleate and grow actin filaments, whereas the heads of the approximately eight Myo2 dimers belonging to a node are represented by an ellipsoid with dimensions and location matching the experimental data. The semiflexible actin filaments are represented by chains of rods with bending stiffness corresponding to the ∼10 µm persistence length (Ott et al., 1993), and Myp2 is represented as unanchored 200 nm

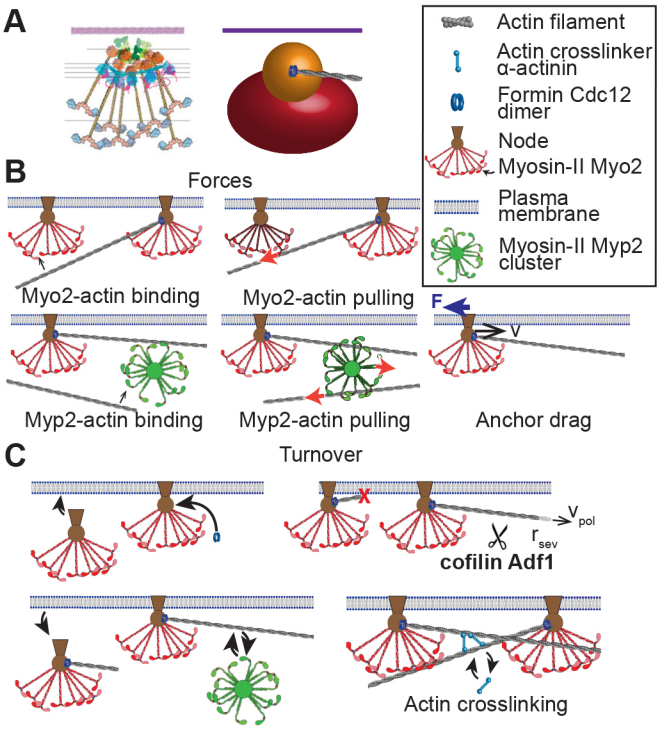

Fig. 1. Molecularly explicit model of the *S. pombe* contractile ring. (A) Left, schematic of membrane-anchored node organization, adapted with permission from Laplante et al. (2016). Plasma membrane, purple; myosin II Myo2 heads, blue; Myo2 C-terminus, light green; Myo2 light chains, pink; formin Cdc12, magenta; IQGAP Rng2, orange; F-BAR Cdc15, light blue; Mid1, dark green. Right, coarse-grained representation of a node in the model. Red ellipsoid positioned 94 nm from the plasma membrane represents the heads of the eight Myo2 dimers. Orange sphere represents Rng2, Cdc15 and other components. (B) Forces in the model. (C) Turnover of ring components. Formin Cdc12 dimers bind nodes 40 nm from the membrane and polymerize randomly oriented actin filaments at rate v_{pol}. Nodes bind to and dissociate from the plasma membrane. The formin Cdc12 dimers bind nodes and polymerize randomly oriented actin filaments at rate v_{pol}. The cofilin Adf1 (scissors) stochastically severs filaments at rate r_{sev}. Myp2 clusters bind and unbind actin filaments.

clusters of 16 molecules each (Alonso-Matilla et al., 2019; Cheffings et al., 2019; Laplante et al., 2015; Takaine et al., 2015).

Filaments intersecting Myo2 or Myp2 clusters bind and are pulled (Fig. 1B), following linear force–velocity relations with total stall forces per cluster of f^{stall}_{Myo2} and f^{stall}_{Myp2}. Drag forces resist lateral motion of the node parallel to the membrane, with a drag coefficient chosen to reproduce the experimental lateral node velocity distribution (Laplante et al., 2016). Steric repulsions prevent crossing of actin filaments. Actin filaments are dynamically crosslinked by Ain1 α-actinin dimers (Wu and Pollard, 2005).

The component amounts follow the experimental values throughout constriction (Courtemanche et al., 2016; Wu and Pollard, 2005). For example, at constriction onset, the ring contains 3300 Myo2 molecules, 230 formin dimers in ∼210 nodes, 2300 Myp2 molecules in ∼140 clusters, and 230 actin filaments of total length ∼580 µm.

On binding a node, a formin nucleates a randomly oriented actin filament. Cofilin-mediated severing stochastically shortens filaments homogenously with rate r_{sev}=0.93 µm^{-1} min^{-1} (see Table 1; Elam et al., 2013). A whole-node turnover scheme is assumed, with a node dissociation time of 41 s, which is consistent with measured dissociation rates of node components. Myp2

Journal of Cell Science (2023) 136, jcs259969. doi:10.1242/jcs.259969

Table 1. Key parameter values of the ring simulation

Symbol	Meaning	Value at onset of constriction	Reference
	Ring binding zone width	0.2 μm	Cortés et al. (2007)
	Initial ring length	11.6 μm	Measured in Pelham and Chang (2002)
	Ring constriction rate	70 nm min^{-1}	Measured in Pelham and Chang (2002)
ρ_{Cdc12p}	Density of formin Cdc12p dimers along the ring	20 μm^{-1}	Courtemanche et al. (2016); Feierbach and Chang (2001); Yonetani et al. (2008)*
ρ_{Myo2}	Density of Myo2 nodes along the ring	18 μm^{-1}	Wu and Pollard (2005); Laplante et al. (2016)*
ρ_{Myp2}	Density of Myp2 clusters along the ring	12.5 μm^{-1}	Wu and Pollard (2005); McDargh et al. (2021)*
k^{off}_{Myo2}	Myo2 off-rate	0.0245 s^{-1}	Pelham and Chang (2002); Clifford et al. (2008); Yonetani et al. (2008)
k^{off}_{Myp2}	Myp2 off-rate	0.026 s^{-1}	Takaine et al. (2015)
f^{stall}_{Myo2}	Myo2 stall force per head	1.75 pN	Fitted in McDargh et al. (2021)
f^{stall}_{Myp2}	Myp2 stall force per head	1.0 pN	Fitted in McDargh et al. (2021)
	Major axis of Myo2 capture zone	132 nm	Laplante et al. (2016)
	Minor axes of Myo2 capture zone	102 nm (both)	Laplante et al. (2016)
	Diameter of Myp2 capture zone	200 nm	Takaine et al. (2015)
$\rho_{actinin}$	Density of α-actinin dimers along the ring	25 μm^{-1}	Wu and Pollard (2005)
$k^{off}_{actinin}$	α-actinin off-rate	3.3 s^{-1}	Li et al. (2016)
r_{sev}	Cofilin-mediated severing rate per unit length on actin filament	0.93 μm^{-1} min^{-1}	Fitted in McDargh et al. (2021)*
v_{pol}	Formin-mediated actin polymerization rate	127 nm s^{-1}	Fitted in McDargh et al. (2021)*
l_p	Actin filament persistence length	10 μm	Ott et al. (1993); Riveline et al. (1997)
γ_{anch}	Anchor drag coefficient per node	500 pN s μm^{-1}	McDargh et al. (2021); Laplante et al. (2016)
$k^{Myp2-Myp2}_{ex}$	Myp2-Myp2 excluded volume spring constant	0.32 pN nm^{-1}	
$k^{Myo2-Myo2}_{ex}$	Myo2-Myo2 excluded volume spring constant	0.12 pN nm^{-1}	
$k^{Anchor-Myp2}_{ex}$	Anchor-Myo2 excluded volume spring constant	0.095 pN nm^{-1}	
$r^{Myp2-Myp2}_0$	Myp2-Myp2 excluded volume cutoff distance	200 nm	
$r^{Myo2-Myo2}_0$	Myo2-Myo2 excluded volume cutoff distance	132 nm	
$r^{Anchor-Myp2}_0$	Anchor-Myp2 excluded volume cutoff distance	202 nm	
f_{act}	Actin-actin excluded volume maximum force	10 pN	
r_{ex}	Actin-actin excluded volume distance	15 nm	
$f_{filament}$	Actin-limited stall force	8 pN	Vavylonis et al. (2008)
f^{Myo2}_{unbind}	Myo2-actin unbinding threshold force	40 pN	Fitted in McDargh et al. (2021)
f^{Myp2}_{unbind}	Myp2-actin unbinding threshold force	30 pN	Fitted in McDargh et al. (2021)
v^0_{myo}	Load-free Myo2/Myp2 velocity	0.24 μm s^{-1}	Calculated in McDargh et al. (2021)
k_x	Crosslinker spring constant	25 pN μm^{-1}	Claessens et al. (2006); Meyer and Aebi (1990)
r_x	Crosslinker rest length	30 nm	Claessens et al. (2006); Meyer and Aebi (1990)
θ_{max}	Maximum angle between new actin filament and ring	30°	

*These parameters were tuned throughout constriction to ensure that the time course of component numbers matched previous experimental measurements.

clusters bind actin filaments with a turnover time of 46 s (Takaine et al., 2015). Rates of severing, binding and actin polymerization are set by demanding simulations reproduce the experimental densities of Myo2, Myp2 and formin and mean actin length, all evolving as constriction progresses (Fig. 1C).

Simulations reproduce forces and structural properties of experimental contractile rings

We ran simulations of the model with a septum growing inwards at 2.4 nm s^{-1} (Thiyagarajan et al., 2015) for ∼25 min. Components were initially randomly positioned in a 200 nm wide circular band representing the membrane lining the inside of the septum. Constriction was initialized after a preliminary 3 min run to allow the ring to self-organize. This dynamic organization maintained itself throughout constriction and reproduced many experimental features (Fig. 2A; Movie 1). Consistent with the experimental data, the actin filaments formed an ∼130 nm thick bundle of ∼47 filaments associated with a 100 nm thick Myo2 ring overlapping a concentric 200 nm thick inner Myp2 ring, separated by ∼26 nm (Laplante et al., 2015, 2016; McDonald et al., 2017; Swulius et al., 2018).

Ring tension was generated by a sliding node mechanism (Fig. 2B), very different to the classic sarcomeric mechanism of striated muscle (Huxley and Niedergerke, 1954; Huxley and Hanson, 1954). When incoming nodes bound the membrane, their formins nucleated actin filaments that were pulled by Myo2 belonging to other nodes. Since the membrane-anchored nodes host about one actin filament on average, they were pulled clockwise or counterclockwise around the ring depending on the actin orientation, with a node velocity distribution closely reproducing that measured using FPALM (Laplante et al., 2016; McDargh et al., 2021 preprint). In this way, filaments with barbed ends anchored to the membrane became tense, and a net ring tension was generated by the ∼200 nodes (at constriction onset) (Fig. 2B). Unanchored Myp2 clusters also contributed by pulling filaments. Ring tensions increased from ∼500 to ∼1000 pN as rings constricted (Fig. 4C), with a mean of ∼740 pN, close to the values measured in live fission yeast protoplasts (McDargh et al., 2021 preprint).

Bridging instabilities are the principal structural threat to the contractile ring

The contractile ring builds a specialized organization from actin, myosin and other components that efficiently exerts centripetal force to drive constriction. For functionality, this organization must be stable over the ∼25 mins of constriction. Our simulations and experiments show that the biggest structural threat originates in the high tensions in filaments, which must bend to form the circular

Journal of Cell Science (2023) 136, jcs259969. doi:10.1242/jcs.259969

bundle at the core of the ring (McDargh et al., 2021 preprint). Energetically, bent tensile filaments prefer to straighten by pulling away from the membrane into straight bridges (Fig. 3A).

Now, the centripetal force per length tending to straighten a segment of a ring of radius R_{ring} and tension T into a bridge is T/R_{ring} (Fig. 3A). Furthermore, the principal ring component anchoring actin to the membrane is the membrane-anchored Myo2, which binds actin filaments abundantly and provides the anchoring force, F_{anchor}, that opposes radial displacement of the actin filaments (McDargh et al., 2021 preprint). Myp2 makes a similar bundling contribution.

Thus, we anticipate bridging will be precipitated by either (1) weakened actin-Myo2 binding (lower F_{anchor}), or (2) increased ring tension T (higher centripetal force T/R_{ring}). To test this, we performed simulations (1) with the temperature-sensitive Myo2-E1 mutant, which binds actin weakly and has minimal ATPase activity (Lord and Pollard, 2004; Stark et al., 2013), and (2) with artificially elevated ring tensions T by using nonphysiologically higher values of f^{stall}_{Myo2} (4-fold increase), the stall force parameter which sets the scale of the forces exerted by Myo2 clusters (see Materials and Methods). Indeed, in both cases, rings suffered significant bridging, with Myp2-containing actin bridges 0.5–1.5 µm in length (Fig. 3B,C). The bridging in simulated *myo2-E1* rings (McDargh et al., 2021 preprint) closely matched bridging observed in live cells of the *myo2-E1* mutant, a vivid demonstration of the instability (Laplante et al., 2015) (Fig. 3C).

Contractile rings in *adf1-M3* mutants with reduced actin severing have longer actin filaments and higher ring tension

ADF/cofilin family proteins promote actin turnover by severing actin filaments (Andrianantoandro and Pollard, 2006; Elam et al., 2013; Pavlov et al., 2007). To study the effects of cofilin, we ran simulations to mimic the *adf1-M3* mutant, which has strongly reduced actin binding and severing activity (Chen and Pollard, 2011), by setting the severing rate to zero, r_{sev}=0. In the model, actin then dissociates only as whole filaments when formins dissociate from nodes (McDargh et al., 2021 preprint) (Fig. 1C).

In *adf1-M3* simulations (Fig. 4A) actin filaments were ∼2-fold longer than in wild-type simulations (Fig. 4B). Furthermore, ring tension was ∼2-fold increased over much of the course of constriction (Fig. 4C). Given reduced severing, longer actin filaments are expected, but the enhanced tension is less obvious. To understand this, we measured tensions in individual actin filaments and found that the maximal tension at the anchored barbed end increased roughly linearly with filament length in wild-type simulations (Fig. 4D). Thus, longer filaments have higher tension, because they are bound by more myosin-II dimers. Since the total ring tension is a sum of all filament contributions over the bundle cross-section (Fig. 2B), the net ring tension is higher with longer filaments (McDargh et al., 2021 preprint).

Simulations reproduce bridging observed in contractile rings of *adf1-M3* mutants

Interestingly, bridging instabilities are seen experimentally for the *adf1-M2* and *adf1-M3* mutants with reduced severing activity (Cheffings et al., 2019) (Fig. 4A). Why reduced severing activity triggers bridging is unknown. Our simulation results above have already provided a strong clue – longer actin filaments lead to higher ring tension T (Fig. 4B–D), and higher tension generates higher centripetal Laplace forces $\sim T/R_{ring}$, which promote bridging (Fig. 3A).

This line of reasoning was indeed confirmed by simulations, which showed dramatic bridging instabilities in simulated cofilin mutants. The simulated bridges were remarkably similar to those observed in live cells (Fig. 4A; Movie 2). As demonstrated in Cheffings et al. (2019), bridges contained Myp2, but not Myo2. Leaving Myo2 behind, bridges pulled away from the membrane and comprised several actin filaments bundled by Myp2, as expected given that Myp2 is unanchored and its localization to the ring depends on actin (Laplante et al., 2015; Takaine et al., 2015). Each bridge had a few tenuous attachments to the ring at the bridge ends, mediated by barbed-end-anchored actin filaments.

Bridge formation is negatively correlated with Myo2 concentration

In experimental images of *adf1-M3* contractile rings, the Myo2 density is clearly lower in regions of the membrane from which a bridge has pulled away (Cheffings et al., 2019) (Fig. 4A).

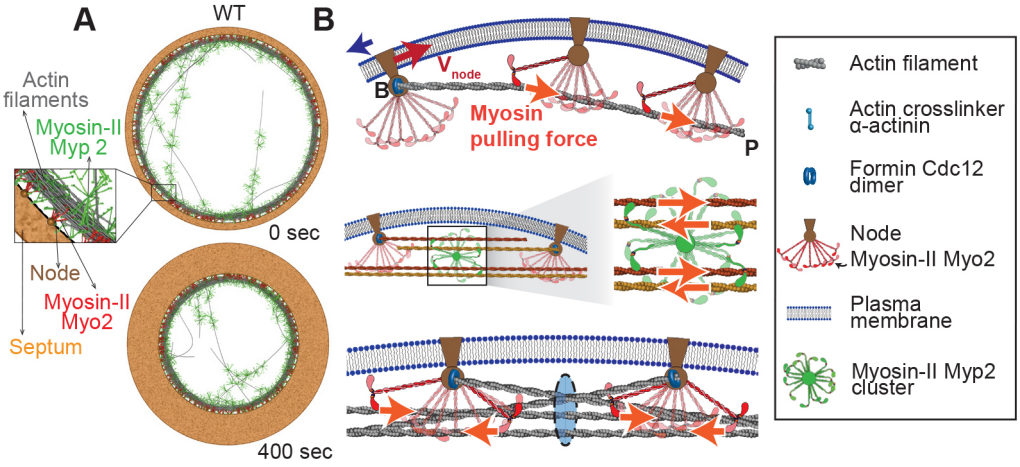

Fig. 2. Sliding node mechanism of ring tension production. Representations of nodes, Myo2, Myp2 and actin filaments are as in Fig. 1. (A) Simulated wild-type (WT) contractile rings at constriction onset and 400 s after onset. The ingrowing septum is shown as the brown region outside the ring. Actin filaments, gray. In images of simulated rings in this and other figures, Myo2 (red) and Myp2 (green) are rendered with explicit molecular detail for clarity. (B) Sliding node ring tension mechanism. Top, individual actin filaments hosted by a node are made tense by pulling forces from Myo2 belonging to other nodes. Filament tension requires drag forces (blue arrow) that oppose motion of the node anchor relative to the membrane. Middle, unanchored Myp2 clusters also contribute to ring tension, by pulling on roughly equal numbers of oppositely oriented actin filaments. Bottom, the sum of the tensions of all actin filaments passing through a given cross-section of the ring gives the net ring tension.

Journal of Cell Science (2023) 136, jcs259969. doi:10.1242/jcs.259969

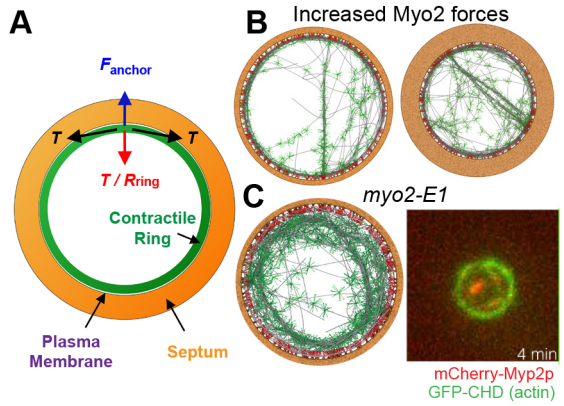

Fig. 3. Mechanism of bridging instability. (A) For a ring of radius R_{ring} the ring tension T produces a centripetal force per unit length T/R_{ring}, normally balanced by anchoring force F_{anchor} provided by membrane-anchored Myo2 belonging to nodes. If Myo2–actin binding is weakened (reduced F_{anchor}, as in *myo2-E1* mutants) or tension is boosted (increased T/R_{ring}, as in cofilin *adf1-M3* mutants) actin filaments might peel off the membrane into straight bridges. (B) Simulations with 4-fold increased Myo2 stall force f^{stall}_{Myo2} show significant bridging. (C) Significant bridging is seen in simulated (McDargh et al., 2021 preprint) and experimental *myo2-E1* rings (4 min from the onset of constriction), where Myo2 heads bind actin weakly. The experimental image is adapted with permission of Elsevier from Laplante et al. (2015); permission conveyed through the Copyright Clearance Center, Inc.

Consistent with these experiments, in simulated cofilin mutants, bridging was more frequent in regions of lower Myo2 density around the ring. Given that Myo2 is hosted by nodes, this was reflected by a negative correlation between node density and bridge location: the node density was ∼2-fold lower in regions of the ring where a bridge occurred than in regions without a bridge (n=30 rings, Fig. 5A; Movie 2).

These experimental and simulation results are consistent with the hypothesis that bridging is a failure of Myo2-mediated anchoring, so that bridging is more likely where fewer anchors are present.

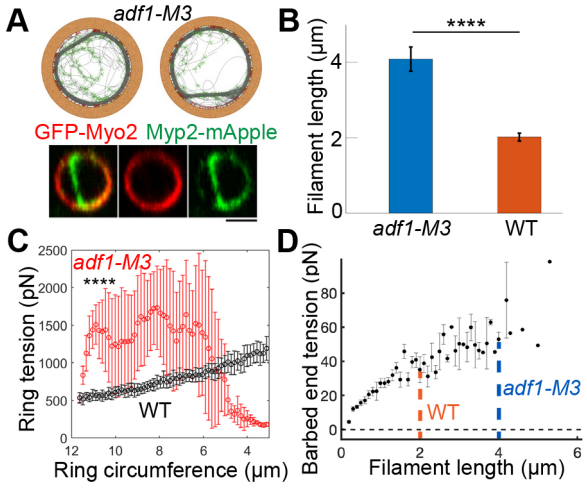

Fig. 4. Bridging instabilities are triggered in cofilin *adf1-M3* mutants because longer actin filaments produce higher ring tension. (A) Simulated *adf1-M3* rings (top row) reproduce bridging observed experimentally in *adf1-M3* mutant cells (bottom row). Simulated and experimental bridges contain Myp2 clusters. Experimental images adapted with permission of American Society for Cell Biology from Cheffings et al. (2019); permission conveyed through Copyright Clearance Center, Inc. Scale bar: 2 µm. (B) Actin filament length (mean±s.d.) in simulated *adf1-M3* (n=30) and wild-type (n=30) rings 500 s after constriction onset. ****P<0.0001 (Welch's unequal variances two-tailed t-test). (C) Ring tensions (mean±s.d.) during constriction in simulated *adf1-M3* (n=30) and wild-type (n=30) rings. ****P<0.0001 (Welch's unequal variances two-tailed t-test for every ring circumference exceeding 8 µm). (D) Actin filament tension at the node-attached barbed end (mean±s.d.) versus filament length in simulated wild-type rings 500 s after constriction onset (n=30). Dashed lines indicate mean lengths of results shown in B.

Simulations reproduce cyclic bridging observed in contractile rings of cofilin mutants

In *adf1-M3* cells, bridging in contractile rings was cyclic with three cycles over the course of ring constriction (Cheffings et al., 2019) (Fig. 5B). Remarkably, our simulations quantitatively reproduced this behavior – fitting our simulated data to a sum of Gaussians using the identical statistical procedure to that used in the experimental study (Cheffings et al., 2019), we find three cycles of bridging and self-assembly occur during constriction (Fig. 5B; Movie 2). Thus, simulations reproduce cyclic bridging and the number of cycles per constriction observed in live cells, although with a somewhat shorter time interval between bridging episodes (∼4.5 min in simulations versus ∼7 min experimentally, Fig. 5B). This might be because the experimental measurements span a longer time period, including the maturation episode that begins ∼20 min before constriction (Wu and Pollard, 2005), whereas all simulations begin at constriction onset (time zero in Fig. 5B).

We argue that the reproduction of this very specific experimental phenotype strongly suggests the simulation recapitulates the essential mechanisms governing the fission yeast contractile ring. In particular, we conclude that the cofilin-mediated turnover that maintains actin filament lengths within a certain range are essential to protect the ring from bridging instability.

DISCUSSION

Here, we studied the role of ADF/cofilin family proteins that sever actin filaments in the contractile ring by simulating rings in cofilin mutants and making detailed comparisons with experiments on the same mutant. Two candidates are the *adf1-M2* and *adf1-M3* mutants. In both mutants, the severing activity of cofilin is reduced but constriction rates are normal (Cheffings et al., 2019; Chen and Pollard, 2011). Adf1-M3 has two mutations (E132A and K133A), binds actin filaments ∼10-fold more slowly than wild-type and severs actin defectively (Chen and Pollard, 2011). In a severing assay (Chen and Pollard, 2011), Adf1-M3 required an ∼10-fold higher concentration than wild-type Adf1 for maximal actin-severing activity, and even then the severing rate was ∼3-fold reduced from wild-type. Thus, to study the effects of cofilin, we ran simulations that mimic the *adf1-M3* mutant in which we set the severing rate to zero, r_{sev}=0.

Our results provide evidence that actin turnover is essential for the structural stability of the actomyosin contractile ring. By regulating the length of actin filaments, ADF/cofilin-mediated severing protects the ring from bridging, its principal structural threat manifested in live cells in *myo2-E1* (Laplante et al., 2015) and *adf1* mutants (Cheffings et al., 2019; Chen and Pollard, 2011). Our modeling results explain why ring disruption due to this instability is expected in these two apparently unrelated contexts – in one case due to weakened anchoring, in the other due to increased unanchoring force.

The principal job of the contractile ring is to generate tension and exert inward centripetal force that directs constriction, accomplished by myosin II pulling on the bundled curved actin filaments in the ring and making them tense. However, a curved actin filament under

Journal of Cell Science (2023) 136, jcs259969. doi:10.1242/jcs.259969

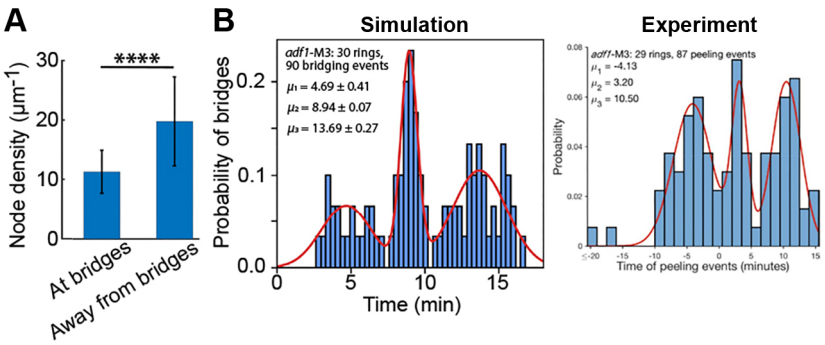

Fig. 5. Simulated *adf1-M3* rings show cyclic bridging and negative correlation of bridging location with local Myo2 concentration. (A) Node density (mean±s.d.) at and away from bridging sites in simulated *adf1-M3* rings (n=20 bridging events). ****P<0.0001 (paired two-tailed t-test). (B) Probability of bridging at different times during constriction of simulated *adf1-M3* rings and of experimental *adf-M3* rings. Image on the right adapted with permission of American Society for Cell Biology from Cheffings et al. (2019); permission conveyed through Copyright Clearance Center, Inc. Histogram shows the number of bridging events in each 20 s time bin divided by total number of bridging events in n=30 simulations (left). Red curves: best fit Gaussian mixture models, three Gaussians with means μ_1, μ_2, μ_3. For the simulations, the best fit widths are 1.68±0.44, 0.56±0.07 and 1.84±0.28 min (mean±s.d.), respectively. Simulation data are for constriction only (0 min and later), whereas experimental data include the maturation episode preceding constriction (negative times).

tension has an enormous energetic preference to become straight. For example, 500 s after constriction onset a typical filament has length $l_{\mathrm{act}} \sim 2\,\mu\mathrm{m}$ and tension $T_{\mathrm{fil}} \sim 15\,\mathrm{pN}$ (Fig. 4B,D) given that the mean filament tension is one half the barbed end value (McDargh et al., 2021 preprint). Given the ring radius of ∼1.3 µm, its end-to-end distance increases by $\Delta L \sim 0.2\,\mu\mathrm{m}$ on straightening, giving an energy advantage whose order of magnitude is $\sim T_{\mathrm{fil}}\Delta L \sim 750\,kT$. Summed over a bundle, this yields an enormous thermodynamic driving force for actin filament bundles in the ring to straighten into bridges. Thus, the contractile ring is vulnerable to straightening instability and must be stabilized by anchoring. We find the principal anchoring agent is the membrane-anchored Myo2, which binds actin filaments (McDargh et al., 2021 preprint) (see Fig. 3A,C).

The contractile ring has presumably evolved to efficiently generate tension T, given the available myosin II in the ring. However, above a certain level tension is structurally dangerous, as the force $\sim T/R_{\mathrm{ring}}$ that powers bridging will exceed the opposing Myo2-mediated anchoring forces. Cofilin-mediated severing plays a critical role because the tension depends on the actin filament length, $T \sim \rho_{\mathrm{myo}}\, l_{\mathrm{act}}$ (McDargh et al., 2021 preprint). Thus, for a given density ρ_{myo} of myosin II along the ring, longer filaments lead to higher ring tension and above a certain length provoke bridging. The principal conclusion of our study is that it is the job of cofilin to prune the actin filaments sufficiently that their length never exceeds this dangerous threshold (Fig. 4B).

Consistent with this conclusion, bridging is more likely in segments of the ring where the Myo2 density is lower. This has been observed in experimental studies of *adf1-M3* contractile rings (Cheffings et al., 2019) (Fig. 4A), and we found the same is true in *adf1-M3* simulations (Fig. 5A). Thus, bridging is a failure of Myo2-mediated anchoring in which tense actin filaments pull away from Myo2 that normally binds them to the membrane. Bridges peel away from the plasma membrane at locations where the inward Laplace forces exceed the local anchoring force from Myo2, which depends on the Myo2–actin unbinding threshold and the number of Myo2 heads that bind filaments. Thus, bridging is most likely in regions with low Myo2 density.

We remark that other conceivable sources of structural instability include fracture of individual actin filaments or filament pull-away from formins, given filament tensions reach tens of piconewtons (Fig. 4D). However, fracture tensions ∼100 pN measured for rabbit skeletal muscle actin filaments (Kishino and Yanagida, 1988) suggest filaments can withstand such loads, and measured formin–actin dissociation constants in budding yeast (Pruyne et al., 2002) and mouse (Harris et al., 2004) are of the order of 10 nM, indicating strong formin-actin barbed end binding.

Actin turnover as a necessary stabilizing process to protect the structure of actomyosin contractile assemblies is an emerging theme. Component turnover has been proposed to allow the fission yeast ring to rapidly reassemble itself without trauma as it gradually constricts (McDargh et al., 2021 preprint), and actin turnover is required for homeostasis of the ring (Chew et al., 2017). In *Drosophila* embryos, actomyosin assemblies driving apical constriction were observed to recoil from adherens junctions when cofilin was inhibited by depleting cofilin phosphatase (Jodoin et al., 2015). Following breakage, the mechanical connections between the actomyosin structures and the adherens junctions were re-established on an ∼2 min timescale (Jodoin et al., 2015). This rupture–repair cycle is reminiscent of the ∼7 min bridging–repair cycles in the fission yeast contractile ring (Cheffings et al., 2019).

MATERIALS AND METHODS

A brief summary of the model of the fission yeast contractile ring is presented below. For further details see McDargh et al. (2021 preprint).

Node organization

The model uses a coarse-grained representation of the membrane-anchored nodes (Laplante et al., 2016) (Fig. 1A). (1) Near the membrane, a sphere represents Cdc15 and IQGAP Rng2, with size and location matching the experimental 70 nm wide Cdc15 distribution; (2) formin Cdc12 dimers, binding the node 44 nm from the membrane, nucleate and grow actin filaments; (3) an ellipsoid with the experimental 132×102×102 nm dimensions located 94 nm from the membrane represents the heads of the approximately eight Myo2 dimers.

Actin filaments

Actin filaments are represented as chains of 100 nm long rods (actin subunits). At the chain hinges, torsional springs impose a bending stiffness consistent with the reported persistence length of ∼10 µm (Ott et al., 1993).

Myosin forces

Actin filaments intersecting Myo2 or Myp2 clusters bind and are pulled parallel to the filament (Fig. 1B). We use linear force–velocity relations for Myo2 and Myp2, with stall forces per cluster, $f^{\mathrm{stall}}_{\mathrm{Myo2}}$ and $f^{\mathrm{stall}}_{\mathrm{Myp2}}$, and with the

measured load-free velocity v^0_{myo} for the estimated 25 myosin II heads per actin filament, $v^0_{myo} = 0.24\ \mu m\ s^{-1}$ (Stark et al., 2010). The same load-free velocity was used for Myp2. The pulling force experienced by the actin filaments captured by a Myo2 node or a Myp2 cluster depends on the number of captured filaments: below a critical number n^* (myosin heads in excess), each filament experiences a maximum force $f_{filament}$=8 pN from a node or cluster; above the critical number n^* (actin filaments in excess), the maximal force of 16 myosin heads is distributed equally among the filaments. The critical number n^*=8.75 is the ratio of the total force exerted by 16 heads, $16f^{stall}_{Myo2/Myp2}$, over the maximum force exerted on a filament.

Actin-myosin binding and unbinding

When an actin filament subunit intersects a Myo2 ellipsoid (132×102×102 nm), it experiences a force perpendicular to the filament segment, pulling the filament towards the center of the ellipsoid. The force depends linearly on the distance between the center of the Myo2 ellipsoid and the actin subunit, with rest length d_{Myo2}=25.5 nm. The spring constant is k_{Myo2}. A similar binding rule is applied to Myp2 clusters, with d_{Myp2}=50 nm, and spring constant k_{Myp2}. The values of these two spring constants were obtained by fitting the unbinding threshold forces of Myo2 and Myp2, f^{Myo2}_{unbind} and f^{Myp2}_{unbind}, to the experimental ring thickness and Myo2–Myp2 separation (McDargh et al., 2021 preprint).

Actin crosslinking

Actin filaments are dynamically crosslinked by Ain1 α-actinin dimers, which act as springs of rest length 30 nm and spring constant 25 pN μm^{-1}, as taken from experimental data (Claessens et al., 2006; Meyer and Aebi, 1990). α-Actinin stochastically binds pairs of actin subunits separated by less than the α-actinin length (30 nm) and unbinds stochastically after a mean time 0.3 s (Li et al., 2016) or when overstretched (length >50 nm).

Drag forces and steric forces

The membrane-anchored nodes experience drag forces resisting lateral motion parallel to the membrane, with a drag coefficient chosen to reproduce the experimental node velocity distribution, whose mean value is 22±10 nm s^{-1} (Laplante et al., 2016). Node–node, Myp2–Myp2, node–Myp2 and actin–actin steric forces oppose overlapping of clusters or filaments. For node–node, Myp2–Myp2 and node–Myp2 interactions, the excluded volume interactions are soft elastic potentials with cut-off scales (see Table 1). Given the typical node–node separation in simulations is ∼50 nm, less than the cut-off scale of node–node interactions (132 nm), Myo2 of adjacent nodes overlaps. These excluded volume interactions between nodes produce an effective node–node friction adding to the node–membrane drag resistance to node motion, a necessary contribution to reproduce the experimental node velocity distribution (Laplante et al., 2016). For the actin–actin interaction, the steric force takes the exponential form with a decay length.

Amounts and turnover of ring components

The component amounts follow the experimental values throughout constriction (Courtemanche et al., 2016; Wu and Pollard, 2005). Given that the detailed kinetics governing the building and dismantling of nodes are unknown, for simplicity the model assumes a whole-node turnover scheme, in which Myo2 binds and dissociates from the ring as a cluster of eight Myo2 dimers together with its host node. The node dissociation time is 41 s, consistent with the measured dissociation times of node components (Clifford et al., 2008; Pelham and Chang, 2002; Yonetani et al., 2008). Nodes stochastically bind a 0.2 μm wide zone, representing the ingrowing septum edge (Cortés et al., 2007), with a binding rate chosen to yield the experimentally determined density of nodes along the ring (Laplante et al., 2016; Wu and Pollard, 2005). On binding a node, a formin nucleates and grows an actin filament that is stochastically shortened by cofilin-mediated severing (Elam et al., 2013). The initial orientation of the nucleated filament is random, within limits such that the orientation is inward and within an angle θ_{max} of the ring direction. Results were insensitive to the nucleated filament orientation distribution. Myp2 clusters bind actin filaments with turnover time 46 s (Takaine et al., 2015). Cofilin-mediated severing stochastically shortens actin filaments homogeneously with rate r_{sev}=0.93 $\mu m^{-1}\ min^{-1}$ (Elam et al., 2013). Rates of binding, actin polymerization and actin filament severing are set by demanding simulations reproduce the experimental densities of Myo2, Myp2 and formin and mean actin length, all evolving as constriction progresses (Courtemanche et al., 2016; Wu and Pollard, 2005).

Running the simulation

A dynamic boundary condition represents the ingrowing septum whose diameter, initially 3.7 μm, decreases at 2.4 nm s^{-1} (Thiyagarajan et al., 2015) for a total constriction time of ∼25 min. The width of the contractile ring is self-determined by the simulation.

Model parameters

Parameters used are shown in Table 1. For simulations with artificially boosted Myo2 forces (Fig. 3B), the stall force f^{stall}_{Myo2} was increased 4-fold, from 1.75 pN to 7 pN. For simulations of *myo2-E1* mutants (Fig. 3C), the Myo2 stall force f^{stall}_{Myo2} was set to zero, and the unbinding threshold f^{Myo2}_{unbind} was reduced from 40 pN to 12 pN. For simulations of *adf1-M3* mutants the severing rate r_{sev} was set to zero.

The density of Myo2 nodes along the ring, ρ_{Myo2}, was calculated from 2900 Myo2p in a 10 μm long ring at the onset of constriction (Wu and Pollard, 2005) and eight Myo2 dimers per node (Laplante et al., 2016), which gives the density of 18 μm^{-1}. Accordingly, The density of Myp2 clusters, ρ_{Myo2}, was calculated from 2000 Myp2p in a 10 μm long ring at the onset of constriction (Wu and Pollard, 2005) and 16 Myp2 heads per cluster, determined in McDargh et al. (2021 preprint), giving the density of 12.5 μm^{-1}.

Myo2 off-rate was determined based on the lifetimes of myosin light chains Cdc4 (Pelham and Chang, 2002) and Rlc1 (Clifford et al., 2008) and the formin Cdc12 (Yonetani et al., 2008), measured previously using FRAP. We calculated the off-rate from the Rlc1 lifetime and used it for the Myo2 off-rate as this was in the middle of the range of experimental values. Myp2 off-rate is consistent with off-rates of 0.022 s^{-1} obtained using previous FRAP measurements of Myp2 (Takaine et al., 2015).

The major axis and the minor axes of Myo2 capture zone were acquired from the distribution of Myo2 heads measured by FPALM (Laplante et al., 2016). The diameter of Myp2 capture zone was acquired from the apparent size of Myp2 clusters measured by deconvolution microscopy (Takaine et al., 2015).

The anchor drag coefficient per node was fitted in McDargh et al. (2021 preprint) to reproduce the node velocity (22±10 nm s^{-1}) measured by FPALM (Laplante et al., 2016).

The crosslinker spring constant and the crosslinker rest length were estimated from *in vitro* measurements on crosslinked actin bundles (Claessens et al., 2006) and from measurements of α-actinin length using electron microscopy (Meyer and Aebi, 1990).

The maximum angle between new actin filaments and the ring was chosen to minimize the fraction of actin in whiskers. The overall structure of the ring was qualitatively insensitive to increases in this parameter, although the whisker fraction increases with larger maximum angles.

Code

All codes (MATLAB) for our molecularly explicit model are available on our public GitHub page (https://github.com/OShaughnessyGroup-Columbia-University/constriction_of_the_fission_yeast_contractile_ring).

Acknowledgements

We thank Mohan Balasubramanian, University of Warwick, for providing experimental images and data of *adf1-M3* rings for comparison. We thank Thomas D. Pollard, Yale University, for providing experimental images of *myo2-E1* rings for comparison. We acknowledge computing resources from Columbia University's Shared Research Computing Facility project.

Competing interests

The authors declare no competing or financial interests.

Author contributions

Conceptualization: B.O.; Methodology: Z.M., B.O.; Formal analysis: Z.M., T.Z., H.Z.; Investigation: Z.M., T.Z., H.Z.; Writing - original draft: B.O.; Writing - review & editing: B.O.; Visualization: T.Z., H.Z.; Supervision: B.O.; Funding acquisition: B.O.

Funding

This work was supported by National Institute of General Medical Sciences of the National Institutes of Health under award number R01GM086731 to B.O. The content is solely the responsibility of the authors and does not necessarily represent the official views of the National Institutes of Health. Deposited in PMC for release after 12 months.

Peer review history

The peer review history is available online at https://journals.biologists.com/jcs/lookup/doi/10.1242/jcs.259969.reviewer-comments.pdf

References

Abe, H., Obinata, T., Minamide, L. S. and Bamburg, J. R. (1996). Xenopus laevis actin-depolymerizing factor/cofilin: a phosphorylation-regulated protein essential for development. *J. Cell Biol.* **132**, 871-885. doi:10.1083/jcb.132.5.871

Alonso-Matilla, R., Thiyagarajan, S. and O'Shaughnessy, B. (2019). Sliding filament and fixed filament mechanisms contribute to ring tension in the cytokinetic contractile ring. *Cytoskeleton* **76**, 611-625. doi:10.1002/cm.21558

Andrianantoandro, E. and Pollard, T. D. (2006). Mechanism of actin filament turnover by severing and nucleation at different concentrations of ADF/cofilin. *Mol. Cell* **24**, 13-23. doi:10.1016/j.molcel.2006.08.006

Bezanilla, M., Forsburg, S. L. and Pollard, T. D. (1997). Identification of a second myosin-II in Schizosaccharomyces pombe: Myp2p is conditionally required for cytokinesis. *Mol. Biol. Cell* **8**, 2693-2705. doi:10.1091/mbc.8.12.2693

Chatterjee, M. and Pollard, T. D. (2019). The functionally important N-terminal half of fission yeast Mid1p anillin is intrinsically disordered and undergoes phase separation. *Biochemistry* **58**, 3031-3041. doi:10.1021/acs.biochem.9b00217

Cheffings, T. H., Burroughs, N. J. and Balasubramanian, M. K. (2019). Actin turnover ensures uniform tension distribution during cytokinetic actomyosin ring contraction. *Mol. Biol. Cell* **30**, 933-941. doi:10.1091/mbc.E18-08-0511

Chen, Q. and Pollard, T. D. (2011). Actin filament severing by cofilin is more important for assembly than constriction of the cytokinetic contractile ring. *J. Cell Biol.* **195**, 485-498. doi:10.1083/jcb.201103067

Chen, Q., Courtemanche, N. and Pollard, T. D. (2015). Aip1 promotes actin filament severing by cofilin and regulates constriction of the cytokinetic contractile ring. *J. Biol. Chem.* **290**, 2289-2300. doi:10.1074/jbc.M114.612978

Chew, T. G., Huang, J., Palani, S., Sommese, R., Kamnev, A., Hatano, T., Gu, Y., Oliferenko, S., Sivaramakrishnan, S. and Balasubramanian, M. K. (2017). Actin turnover maintains actin filament homeostasis during cytokinetic ring contraction. *J. Cell Biol.* **216**, 2657-2667. doi:10.1083/jcb.201701104

Claessens, M. M., Bathe, M., Frey, E. and Bausch, A. R. (2006). Actin-binding proteins sensitively mediate F-actin bundle stiffness. *Nat. Mater.* **5**, 748-753. doi:10.1038/nmat1718

Clifford, D. M., Wolfe, B. A., Roberts-Galbraith, R. H., McDonald, W. H., Yates, J. R., III and Gould, K. L. (2008). The Clp1/Cdc14 phosphatase contributes to the robustness of cytokinesis by association with anillin-related Mid1. *J. Cell Biol.* **181**, 79-88. doi:10.1083/jcb.200709060

Cortés, J. C., Konomi, M., Martins, I. M., Muñoz, J., Moreno, M. B., Osumi, M., Duran, A. and Ribas, J. C. (2007). The (1,3)β-d-glucan synthase subunit Bgs1p is responsible for the fission yeast primary septum formation. *Mol. Microbiol.* **65**, 201-217. doi:10.1111/j.1365-2958.2007.05784.x

Courtemanche, N., Pollard, T. D. and Chen, Q. (2016). Avoiding artefacts when counting polymerized actin in live cells with LifeAct fused to fluorescent proteins. *Nat. Cell Biol.* **18**, 676-683. doi:10.1038/ncb3351

D'Avino, P. P., Giansanti, M. G. and Petronczki, M. (2015). Cytokinesis in animal cells. *Cold Spring Harb. Perspect. Biol.* **7**, a015834. doi:10.1101/cshperspect.a015834

Elam, W. A., Kang, H. and De la Cruz, E. M. (2013). Biophysics of actin filament severing by cofilin. *FEBS Lett.* **587**, 1215-1219. doi:10.1016/j.febslet.2013.01.062

Feierbach, B. and Chang, F. (2001). Roles of the fission yeast formin for3p in cell polarity, actin cable formation and symmetric cell division. *Curr. Biol.* **11**, 1656-1665. doi:10.1016/S0960-9822(01)00525-5

Friend, J. E., Sayyad, W. A., Arasada, R., McCormick, C. D., Heuser, J. E. and Pollard, T. D. (2018). Fission yeast Myo2: molecular organization and diffusion in the cytoplasm. *Cytoskeleton* **75**, 164-173. doi:10.1002/cm.21425

Glotzer, M. (2005). The molecular requirements for cytokinesis. *Science* **307**, 1735-1739. doi:10.1126/science.1096896

Gunsalus, K. C., Bonaccorsi, S., Williams, E., Verni, F., Gatti, M. and Goldberg, M. L. (1995). Mutations in twinstar, a Drosophila gene encoding a cofilin/ADF homologue, result in defects in centrosome migration and cytokinesis. *J. Cell Biol.* **131**, 1243-1259. doi:10.1083/jcb.131.5.1243

Harris, E. S., Li, F. and Higgs, H. N. (2004). The mouse formin, FRLα, slows actin filament barbed end elongation, competes with capping protein, accelerates polymerization from monomers, and severs filaments. *J. Biol. Chem.* **279**, 20076-20087. doi:10.1074/jbc.M312718200

Hayakawa, Y., Takaine, M., Imai, T., Yamada, M. D., Hirose, K., Ngo, K. X., Kodera, N., Tokuraku, K., Numata, O., Nakano, K. et al. (2020). Actin binding domain of Rng2 strongly inhibits actin movement on myosin II HMM through structural changes of actin filaments. *bioRxiv 2020.04.14.041046*. doi:10.1101/2020.04.14.041046

Huxley, H. and Hanson, J. (1954). Changes in the cross-striations of muscle during contraction and stretch and their structural interpretation. *Nature* **173**, 973-976. doi:10.1038/173973a0

Huxley, A. F. and Niedergerke, R. (1954). Structural changes in muscle during contraction: interference microscopy of living muscle fibres. *Nature* **173**, 971-973. doi:10.1038/173971a0

Jodoin, J. N., Coravos, J. S., Chanet, S., Vasquez, C. G., Tworoger, M., Kingston, E. R., Perkins, L. A., Perrimon, N. and Martin, A. C. (2015). Stable force balance between epithelial cells arises from F-actin turnover. *Dev. Cell* **35**, 685-697. doi:10.1016/j.devcel.2015.11.018

Kishino, A. and Yanagida, T. (1988). Force measurements by micromanipulation of a single actin filament by glass needles. *Nature* **334**, 74-76. doi:10.1038/334074a0

Laplante, C., Berro, J., Karatekin, E., Hernandez-Leyva, A., Lee, R. and Pollard, T. D. (2015). Three myosins contribute uniquely to the assembly and constriction of the fission yeast cytokinetic contractile ring. *Curr. Biol.* **25**, 1955-1965. doi:10.1016/j.cub.2015.06.018

Laplante, C., Huang, F., Tebbs, I. R., Bewersdorf, J. and Pollard, T. D. (2016). Molecular organization of cytokinesis nodes and contractile rings by super-resolution fluorescence microscopy of live fission yeast. *Proc. Natl. Acad. Sci. USA* **113**, E5876-E5885. doi:10.1073/pnas.1608252113

Li, Y. J., Christensen, J. R., Homa, K. E., Hocky, G. M., Fok, A., Sees, J. A., Voth, G. A. and Kovar, D. R. (2016). The F-actin bundler α-actinin Ain1 is tailored for ring assembly and constriction during cytokinesis in fission yeast. *Mol. Biol. Cell* **27**, 1821-1833. doi:10.1091/mbc.e16-01-0010

Lord, M. and Pollard, T. D. (2004). UCS protein Rng3p activates actin filament gliding by fission yeast myosin-II. *J. Cell Biol.* **167**, 315-325. doi:10.1083/jcb.200404045

Malla, M., Pollard, T. D. and Chen, Q. (2022). Counting actin in contractile rings reveals novel contributions of cofilin and type II myosins to fission yeast cytokinesis. *Mol. Biol. Cell* **33**, ar51. doi:10.1091/mbc.E21-08-0376

McDargh, Z., Wang, S., Chin, H. F., Thiyagarajan, S., Karatekin, E., Pollard, T. D. and O'Shaughnessy, B. (2021). Myosins generate contractile force and maintain organization in the cytokinetic contractile ring. *bioRxiv, 2021.05.02.442363*. doi:10.1101/2021.05.02.442363

McDonald, N. A., Lind, A. L., Smith, S. E., Li, R. and Gould, K. L. (2017). Nanoscale architecture of the Schizosaccharomyces pombe contractile ring. *Elife* **6**, e28865. doi:10.7554/eLife.28865

Meyer, R. K. and Aebi, U. (1990). Bundling of actin filaments by alpha-actinin depends on its molecular length. *J. Cell Biol.* **110**, 2013-2024. doi:10.1083/jcb.110.6.2013

Nakano, K. and Mabuchi, I. (2006). Actin-depolymerizing protein Adf1 is required for formation and maintenance of the contractile ring during cytokinesis in fission yeast. *Mol. Biol. Cell* **17**, 1933-1945. doi:10.1091/mbc.e05-09-0900

O'Shaughnessy, B. and Thiyagarajan, S. (2018). Mechanisms of contractile ring tension production and constriction. *Biophys. Rev.* **10**, 1667-1681. doi:10.1007/s12551-018-0476-6

Ono, K., Parast, M., Alberico, C., Benian, G. M. and Ono, S. (2003). Specific requirement for two ADF/cofilin isoforms in distinct actin-dependent processes in Caenorhabditis elegans. *J. Cell Sci.* **116**, 2073-2085. doi:10.1242/jcs.00421

Ott, A., Magnasco, M., Simon, A. and Libchaber, A. (1993). Measurement of the persistence length of polymerized actin using fluorescence microscopy. *Phys. Rev. E Stat. Phys. Plasmas Fluids Relat. Interdiscip. Topics* **48**, R1642-R1645. doi:10.1103/physreve.48.r1642

Pavlov, D., Muhlrad, A., Cooper, J., Wear, M. and Reisler, E. (2007). Actin filament severing by cofilin. *J. Mol. Biol.* **365**, 1350-1358. doi:10.1016/j.jmb.2006.10.102

Pelham, R. J. and Chang, F. (2002). Actin dynamics in the contractile ring during cytokinesis in fission yeast. *Nature* **419**, 82-86. doi:10.1038/nature00999

Pollard, T. D. (2007). Regulation of actin filament assembly by Arp2/3 complex and formins. *Annu. Rev. Biophys. Biomol. Struct.* **36**, 451-477. doi:10.1146/annurev.biophys.35.040405.101936

Pollard, T. D. and O'Shaughnessy, B. (2019). Molecular mechanism of cytokinesis. *Annu. Rev. Biochem.* **88**, 661-689. doi:10.1146/annurev-biochem-062917-012530

Pollard, T. D. and Wu, J.-Q. (2010). Understanding cytokinesis: lessons from fission yeast. *Nat. Rev. Mol. Cell Biol.* **11**, 149-155. doi:10.1038/nrm2834

Pollard, L. W., Bookwalter, C. S., Tang, Q., Krementsova, E. B., Trybus, K. M. and Lowey, S. (2017). Fission yeast myosin Myo2 is down-regulated in actin affinity by light chain phosphorylation. *Proc. Natl. Acad. Sci. USA* **114**, E7236-E7244. doi:10.1073/pnas.1703161114

Pruyne, D., Evangelista, M., Yang, C., Bi, E., Zigmond, S., Bretscher, A. and Boone, C. (2002). Role of formins in actin assembly: nucleation and barbed-end association. *Science* **297**, 612-615. doi:10.1126/science.1072309

Riveline, D., Wiggins, C. H., Goldstein, R. E. and Ott, A. (1997). Elastohydrodynamic study of actin filaments using fluorescence microscopy. *Phys. Rev. E* **56**, R1330-R1333. doi:10.1103/PhysRevE.56.R1330

Stachowiak, M. R., Laplante, C., Chin, H. F., Guirao, B., Karatekin, E., Pollard, T. D. and O'Shaughnessy, B. (2014). Mechanism of cytokinetic contractile ring constriction in fission yeast. *Dev. Cell* **29**, 547-561. doi:10.1016/j.devcel.2014.04.021

Stark, B. C., Sladewski, T. E., Pollard, L. W. and Lord, M. (2010). Tropomyosin and myosin-II cellular levels promote actomyosin ring assembly in fission yeast. *Mol. Biol. Cell* **21**, 989-1000. doi:10.1091/mbc.e09-10-0852

Stark, B. C., James, M. L., Pollard, L. W., Sirotkin, V. and Lord, M. (2013). UCS protein Rng3p is essential for myosin-II motor activity during cytokinesis in fission yeast. *PLoS One* **8**, e79593. doi:10.1371/journal.pone.0079593

Swulius, M. T., Nguyen, L. T., Ladinsky, M. S., Ortega, D. R., Aich, S., Mishra, M. and Jensen, G. J. (2018). Structure of the fission yeast actomyosin ring during constriction. *Proc. Natl. Acad. Sci. USA* **115**, E1455-E1464. doi:10.1073/pnas.1711218115

Takaine, M., Numata, O. and Nakano, K. (2015). An actin-myosin-II interaction is involved in maintaining the contractile ring in fission yeast. *J. Cell Sci.* **128**, 2903-2918. doi:10.1242/jcs.171264

Thiyagarajan, S., Munteanu, E. L., Arasada, R., Pollard, T. D. and O'Shaughnessy, B. (2015). The fission yeast cytokinetic contractile ring regulates septum shape and closure. *J. Cell Sci.* **128**, 3672-3681. doi:10.1242/jcs.166926

Thiyagarajan, S., Wang, S. and O'Shaughnessy, B. (2017). A node organization in the actomyosin contractile ring generates tension and aids stability. *Mol. Biol. Cell* **28**, 3286-3297. doi:10.1091/mbc.e17-06-0386

Vavylonis, D., Wu, J. Q., Hao, S., O'Shaughnessy, B. and Pollard, T. D. (2008). Assembly mechanism of the contractile ring for cytokinesis by fission yeast. *Science* **319**, 97-100. doi:10.1126/science.1151086

Wu, J.-Q. and Pollard, T. D. (2005). Counting cytokinesis proteins globally and locally in fission yeast. *Science* **310**, 310-314. doi:10.1126/science.1113230

Wu, J.-Q., Sirotkin, V., Kovar, D. R., Lord, M., Beltzner, C. C., Kuhn, J. R. and Pollard, T. D. (2006). Assembly of the cytokinetic contractile ring from a broad band of nodes in fission yeast. *J. Cell Biol.* **174**, 391-402. doi:10.1083/jcb.200602032

Yonetani, A., Lustig, R. J., Moseley, J. B., Takeda, T., Goode, B. L. and Chang, F. (2008). Regulation and targeting of the fission yeast formin cdc12p in cytokinesis. *Mol. Biol. Cell* **19**, 2208-2219. doi:10.1091/mbc.e07-07-0731

Zhou, Z., Munteanu, E. L., He, J., Ursell, T., Bathe, M., Huang, K. C. and Chang, F. (2015). The contractile ring coordinates curvature-dependent septum assembly during fission yeast cytokinesis. *Mol. Biol. Cell* **26**, 78-90. doi:10.1091/mbc.e14-10-1441

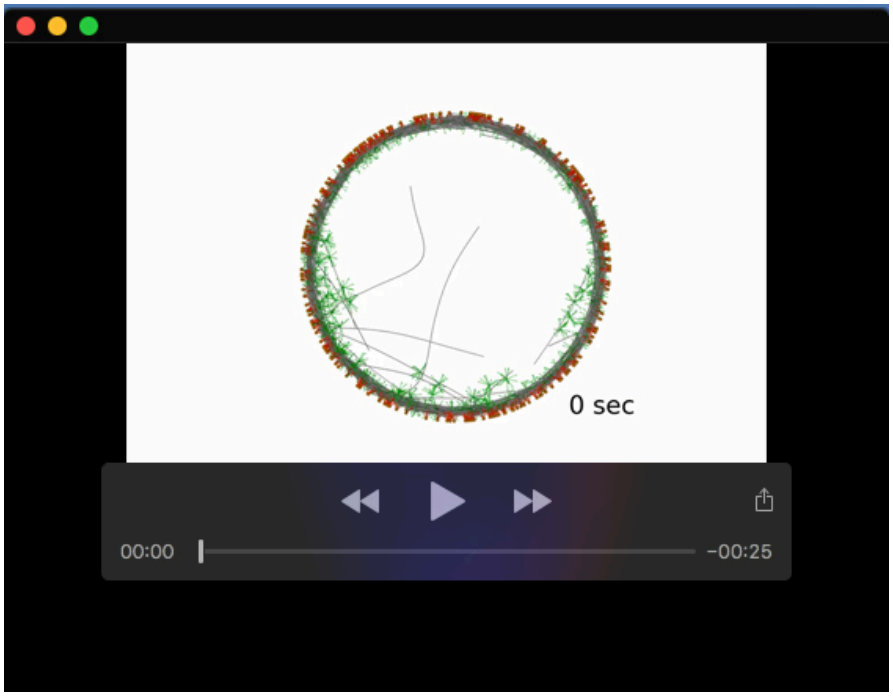

Movie 1. Simulation of a constricting wild-type ring. Components represented according to scheme of Figs. 1, 2. No bridging occurs.

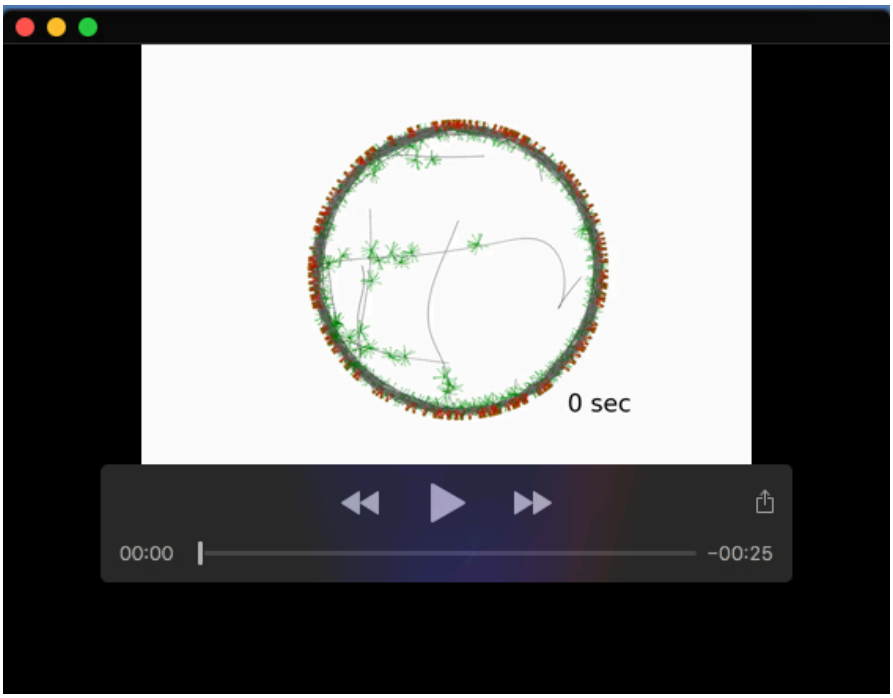

Movie 2. Simulation of a constricting *adf1-M3* ring. Three bridging events occur during constriction (arrows).